Sensing the framework state and guest molecules in MIL-53(Al) via the electron paramagnetic resonance spectrum of V^{IV} dopant ions

Irena Nevjestić[a], Hannes Depauw[b], Peter Gast[c], Pieter Tack[d], Davy Deduytsche[a], Karen Leus[b], Melissa Van Landeghem[e], Etienne Goovaerts[e], Laszlo Vincze[d], Christophe Detavernier[a], Pascal Van Der Voort[b], Freddy Callens[a], Henk Vrielinck[a]

[a] *Department of Solid State Sciences, Ghent University, Krijgslaan 281-S1, B-9000 Gent, Belgium. Fax: 32 9264 4996 ; Tel: 32 9264 4356; E-mail: henk.vrielinck@ugent.be*
[b] *Department of Inorganic and Physical Chemistry, Ghent University, Krijgslaan 281-S3, B-9000 Gent, Belgium.*
[c] *Department of Physics, Leiden University, PO Box 9504, 2300 RA Leiden, The Netherlands.*
[d] *Department of Analytical Chemistry, Ghent University, Krijgslaan 281-S12, B-9000 Gent, Belgium.*
[e] *Department of Physics, University of Antwerp, Universiteitsplein 1, B-2610 Antwerp, Belgium*

X-ray diffraction (XRD) and electron paramagnetic resonance spectroscopy (EPR) were combined to study the structural transformations induced by temperature, pressure and air humidity of the "breathing" metal-organic framework (MOF) MIL-53(Al), doped with paramagnetic V^{IV} ions, after activation. The correlation between *in situ* XRD and thermogravimetric analysis measurements showed that upon heating this MOF in air, starting from ambient temperature and pressure, the narrow pore framework first dehydrates and after that makes the transition to a large pore state (**lp**). The EPR spectra of V^{IV}=O molecular ions, replacing Al-OH in the structure, also allow to distinguish the as synthesized, hydrated (**np-h**) and dehydrated narrow pore (**np-d**), and **lp** states of MIL-53(Al). A careful analysis of EPR spectra recorded at microwave frequencies between 9.5 and 275 GHz demonstrates that all V^{IV}=O in the **np-d** and **lp** states are equivalent, whereas in the **np-h** state (at least two) slightly different V^{IV}=O sites exist. Moreover, the **lp** MIL-53(Al) framework is accessible to oxygen, leading to a notable broadening of the V^{IV}=O EPR spectrum at pressures of a few mbar, while such effect is absent for the **np-h** and **np-d** states for pressures up to 1 bar.

1 Introduction

Metal-Organic Frameworks (MOFs) or porous coordination networks represent a new stage of development of porous materials because of the possibility of tuning their structure to well-defined properties. Characteristics of these self-assembling modular compounds, like pore size, internal surface area or thermal stability can be modified by employing different metal ions and/or organic linkers connecting them. The interest in MOFs has arisen from their numerous possible applications, including gas storage[1,2] and separation[3], sensing[4,5], catalysis[6,7], drug storage and delivery.[8] The breathing phenomenon observed for certain MOFs is characterized by a reversible structural transformation between two or more states upon exposing the framework to external physical or chemical stimuli, resulting in expansion or contraction of the complete framework. Among the breathing MOFs MIL-53 [MIL = Materials of the Institute Lavoisier] is one of the most widely studied and best known materials because of the pronounced changes in its structure when exposed to temperature or gas pressure.[9] Nevertheless, the breathing effect in the MIL-53 family is still far from completely understood. A complicating and intriguing factor is that the flexibility of the MIL-53 framework strongly depends on the nature of the metal site. MIL-53(M) (M=Cr, Al, Ga, Sc, Fe) is constructed from chains of trans-corner-sharing $MO_4(OH)_2$ octahedra, in the other two dimensions connected with terephthalate (also known as 1,4-benzenedicarboxylate (BDC)), forming a 3D ordered network.[9] In the as-synthesized state (MIL-53(Al) **as**) this framework is not flexible because unreacted linker and solvent molecules block the pores. After activation by solvent extraction[10] or by calcination, the MIL-53 framework exhibits a phase transition between a monoclinic hydrated narrow pore state (**np-h**, **np**=narrow pore), characterized by contracted pores due to water uptake in ambient conditions, and an orthorhombic large pore (**lp**) state as a result of dehydration or large uptake of certain gases[9,11]. For certain MIL-53(M) lattices completely and partially dehydrated **np** states have also been reported in literature. In water-free conditions, the transition between **np** and **lp** states induced by temperature without the aid of gas molecules was reported to exhibit a very large hysteresis.[12]. For this reason the **np** state is often referred to as lt (low temperature) and the **lp** as ht (high temperature) in literature. A concise overview of the various (de)hydrated **np** and **lp** states for MIL-53(M) lattices is given in Figure 1.

This paper focuses on MIL-53(Al). The transition of this framework between a **np-h** (originally labelled LT) and a water-free **lp** structure (HT) was first reported by Loiseau *et al.*[9] Liu *et al.* investigated a dehydrated **np** (**np-d**) state of this framework using elastic neutron scattering.[12] This state was obtained by keeping the **np-h** MIL-53(Al) for long time under high vacuum at 395 K. Volkringer *et al.*[13] suggested that the **np-d** state can also be obtained by heating in air.

Here we provide further details about the transition between these states of MIL-53(Al) by combining electron paramagnetic resonance (EPR) spectroscopy with *in situ* X-ray diffraction (XRD). In order to allow EPR studies, we have doped MIL-53(Al) with low concentrations (1-5%) of vanadium. In previous studies we have shown that our solvothermal synthesis method leads to incorporation of V in the metal nodes[14], and that after activation transitions between **np** and **lp** states of the framework can be

monitored via the X-band (9.5 GHz) EPR spectrum of the V^{IV}=O dopant centres.[15] Here we show that multi-frequency EPR also allows to monitor the hydration state of the framework. We present a spin-Hamiltonian analysis for the V^{IV}=O centres in all states and combine EPR intensity measurements with X-ray Absorption Near Edge Structure (XANES) to follow the V valence state in various stages of activation after synthesis. Finally, we show that the V^{IV}=O EPR spectrum is sensitive to O_2 in the framework.

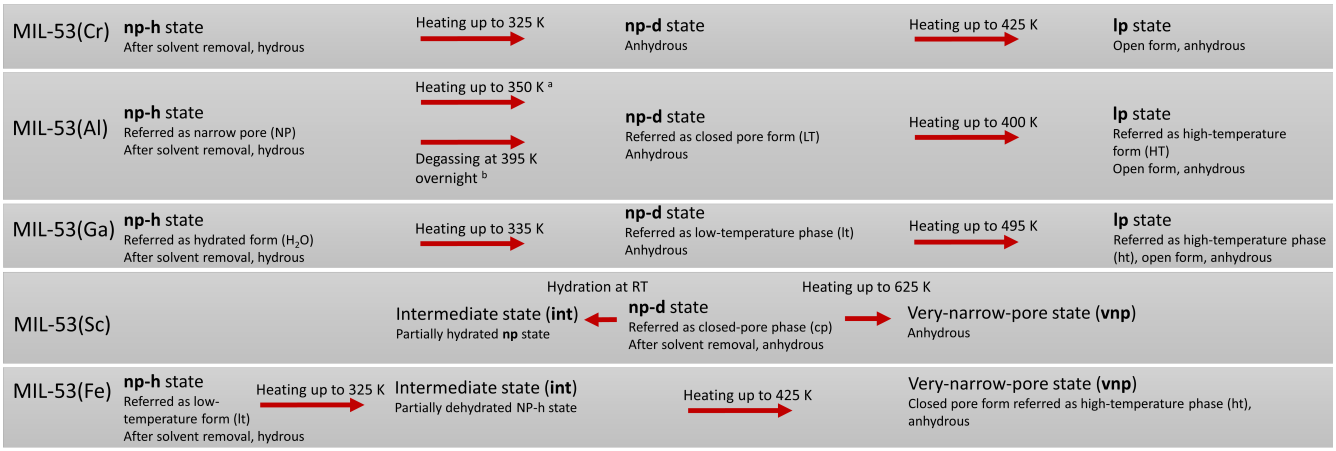

Fig. 1 Overview of the various (de)hydrated **np** and **lp** states for MIL-53(Cr)[16], MIL-53(Al) a[15] and b[12], MIL-53(Ga)[13], MIL-53(Sc)[17] and MIL-53(Fe)[18] lattices obtained by heating and/or evacuating, starting from ambient conditions.

2 Materials and methods

2.1 Synthesis and material characterization of V-doped MIL-53(Al)

Synthesis, powder XRD and N_2 sorption measurements were carried out as previously reported by Nevjestić *et al.*[15] The molar composition of the starting mixtures is presented in Table 1. All samples were synthesized with VCl_3 as dopant salt. Of each sample, a part was activated for further material characterization. We applied a solvent extraction method for activation[10], during which the unreacted linker and metal salts were removed. This procedure consists of three steps. First, the solid is heated at 423 K with dimethylformamide (DMF) in a Teflon-lined autoclave for 24 h. Secondly, the solid is treated at 393 K in methanol for 72 h. Finally, the powder is dried at 473 K for 2 h under vacuum for a complete activation. Samples 5-7 were also activated by calcination. For the calcination procedure, 0.2 gram of **as** sample is spread over the surface of a ceramic plate and heated in a muffle furnace at 573 K for 72 h under air. After activation the samples were collected and stored under dry argon atmosphere. Powder XRD patterns of the reported samples are presented in Figure S1 of the ESI† together with N_2 sorption measurements in Figure S2. A Varian FS-220 F-AAS (Flame Atomic Absorption Spectroscopy) with a nitrous oxide-acetylene flame was used to determine the V/Al atomic concentration ratios in the samples after activation together with a Perkin Elmer Elan DRC 6000 ICP-MS (inductively coupled mass spectroscopy) to determine the vanadium content and a Varian Vista MPX ICP-OES (inductively cou-

pled plasma optical emission spectroscopy) to measure the Al content. To avoid interference with ClO^- anions, during the analysis of vanadium, methane was added as a reaction gas. Before the analysis, the MOF powders were destroyed in an acidic medium. Samples with low vanadium concentrations (0.55 - 4.71 %) were used for EPR in order to obtain a paramagnetically diluted environment.

Table 1 Composition and Langmuir surface area of reported samples. Columns 2 and 3 report concentrations in the starting mixture for synthesis, in the column 4 the [V]/([V]+[Al]) concentration ratios are shown.

Sample *no*.	V-salt (mmol)	Al-salt (mmol)	V (mol %)	Langmuir S. A.
1	0.0814	8.2173	1.47	1527 (m^2/g)
2	0.2797	5.3172	2.56	1542 (m^2/g)
3	0.1118	5.4867	1.48	1494 (m^2/g)
4	0.0559	5.3172	0.55	1520 (m^2/g)
5	0.0559	5.5422	0.57	1488 (m^2/g)
6	0.1118	5.4867	1.65	1536 (m^2/g)
7	0.2797	5.3172	4.71	1462 (m^2/g)
8	0.0559	5.5422	0.62	1538 (m^2/g)

2.2 EPR measurements and analysis

All EPR and Electron Nuclear Double Resonance (ENDOR) measurements were recorded in continuous wave (CW) mode. EPR spectra have been recorded in 4 microwave frequency bands: X-band (∼9.5 GHz), Q-band (∼34 GHz), W-band (∼94 GHz), and J-band (∼275 GHz). Unless otherwise mentioned EPR spectra were mesured at room tempeature (RT). The X-band setup is a Bruker ESP300E spectrometer equipped with an ER 4102ST standard resonator or ER 4114HT high temperature resonator, a HP5350 B frequency counter and a Bruker ER 035M Gaussmeter. The magnetic fields were calibrated using the spectrum of diphenyl picryl hydrazyl (DPPH, g = 2.0036). Q-band EPR and ENDOR spectra were recorded using a Bruker ElexSys E500 spectrometer equipped with a CF910 He-flow cryostat (2-300 K, Oxford Instruments), a Pendulum CNT-90XL frequency counter and a Bruker ER035 M Gaussmeter. The magnetic fields were calibrated against the $g_\perp$ component of the CO_3^{3-} radical in irradiated calcite powder ($g_\perp$= 2.0031)[19]. X- and Q-band EPR spectra were recorded at approximately 5 mW microwave power (avoiding saturation) and 100 kHz modulation. For the W-band (94 GHz) measurements a Bruker ElexSys E680 setup was used (100 kHz modulation frequency, 90 μW microwave power). In X, Q and W-band EPR experiments, small modulation amplitudes were applied (0.1 - 0.4 mT). J-band (275.7 GHz) EPR spectra were obtained on a spectrometer developed at the Huygens Laboratory of Leiden University.[20] The applied microwave power was in the μW range and a modulation amplitude of 1.2 mT at 1.7 kHz modulation frequency was used. Simulations of EPR spectra were performed using the Easyspin toolbox (version 5.1.8) for Matlab[21] by diagonalization of the spin-Hamiltonian

$$\hat{H} = \mu_B \hat{\vec{S}} \cdot \tilde{g} \cdot \vec{B} + \hat{\vec{I}} \cdot \tilde{A} \cdot \hat{\vec{S}} - g_n \mu_N \hat{\vec{I}} \cdot \vec{B} \quad (1)$$

in which μ_B and μ_N represent the Bohr and nuclear magnetons, respectively. For consistency with our previous work, the relative Euler angles for ^{51}V hyperfine tensor (A) with respect to the g tensor presented in this paper have been converted to definitions used in earlier Easyspin versions.[14]

The X-band EPR spectrum of V^{IV} in the **lp** state was recorded after a heating step. The powder sample was placed in a one-end closed quartz capillary (3 mm inner diameter), evacuated by continuous pumping ($\sim$0.01 mbar with a rotary pump) and heated up to 450 K. The sample was then cooled down to RT in vacuum and 1000 mbar of N_2 gas was introduced into the sample tube at RT. For Q and W-band EPR spectra of the **lp** state samples were placed in one-end closed capillaries, heated in a N_2 glove box at 400 K for 2h and sealed with Parafilm (Q-band tube) and wax (W-band tube). EPR spectra were then recorded under He gas flow to avoid oxygen and air humidity.

The spectra of the **np-d** state were recorded in X-band on powder in a one-end closed quartz capillary, evacuated by continuous pumping (at least 2 hours). Powders in Q-band sample tubes were evacuated in a glove box and sealed with Parafilm, the spectra were recorded under He gas flow to avoid oxygen and air humidity. For the J-band measurments quartz sample tubes were open at one end. The microwave cavity and waveguide assembly were placed into a bath cryostat that was flushed two times with nitrogen gas to reduce contributions of molecular oxygen.[22] Spectra were recorded at 325 K and $6\text{x}10^{-3}$ mbar vacuum.

The X, Q and W-band **np-h** state EPR spectra were recorded in air, the J-band spectra in N_2 atmosphere. In order to bring the MOF in this state a closed sample tube containing powder in air was immersed in liquid nitrogen for 12 h, and warmed up to RT short time before measurements.

For X-band EPR measurements as a function of O_2 pressure, the spectra were recorded after a heating step described above to induce the **lp** state. The sample was cooled down to RT in vacuum and compressed O_2 from a gas cylinder was directly connected to the sample tube and introduced in steps of approximately 10 mbar. An EPR spectrum was recorded after each step. The linewidth of the EPR spectra was determined by simulations with the parameters reported for the **lp** state (see Table 3 in section 3.3) and additionally fitting the linewidth (full width at half maximum) with Lorentzian isotropic broadening using the Easyspin toolbox for Matlab.[21]

2.3 *In situ* XRD

In situ powder XRD in air was carried out on a Bruker D8 Discover XRD system equipped with a Cu X-ray source (λ = 1.5406 Å) and a linear X-ray detector. The powder sample was spread on a silicon wafer and placed on the sample heating stage. θ-2θ measurements were carried out in air at atmospheric pressure. The sample was heated from RT to 450 K and cooled back to RT at a heating/cooling rate of 5 K/min. The temperature was measured with a K-type thermocouple. Data were collected in ramping mode with a scanning time of 10 s.

In situ powder XRD in vacuum was carried out on a similar Bruker D8 discover XRD system. The powder sample was placed in a home built reaction chamber and pumped via a manual angle valve with a rotation pump to a pressure of 0.1 mbar. While pumping, the sample was continuously illuminated with X-rays and data was collected via a linear detector.

2.4 Thermogravimetric analysis (TGA)

Thermogravimetric analysis (TGA) data were collected on a Netzsch STA-409CD thermal analyser in a temperature range of 300-460 K under air atmosphere at a heating rate of 2 K/min. At the start of the experiment, V-doped MIL-53(Al) was at RT and had been exposed to (humid) air for considerable time. For the measurements on the **np-d** state the sample was kept under vacuum (10^{-4} mbar) at RT for 48 h prior to the measurements to ensure all water was removed from the structure.

2.5 X-ray absorption near-edge structure spectroscopy (XANES)

XANES was performed at the ESRF (European Synchrotron Radiation Facility, Grenoble, France), beamline BM26A-DUBBLE (Dutch-Belgian Beamline). This 0.4 T bending magnet beamline utilizes a Si(111) monochromator, rendering an X-ray beam flux of approximately $1x10^{10}$ photons/s and an energy resolution $\Delta E/E$ of $1.7x10^{-4}$ at 9.689 keV.[23] Measurements were performed in a He-filled cryostat (Oxford Instruments) at 80 K. The samples were prepared and analysed as pressed pellets, containing a mixture of MOF and cellulose as a binding agent, providing a theoretical absorption of two absorption lengths for 5515 eV X-ray photons. XANES scans were performed over the V K-edge (E_0: 5465 eV) with steps of 0.3 eV over the pre-edge peak and edge regions. Multiple scans were performed to obtain better data quality. XANES data were normalized and processed using the UGent Athena software package. A pseudo-Voigt function was fitted to the pre-edge peak, corresponding to the 1s - 3d electron transition, after subtracting an error function corresponding to the rising edge.

3 Results and discussion

3.1 Three distinct states of activated V-doped MIL-53(Al)

We have previously reported the *in situ* observation with XRD of the transition from the **np** to the **lp** state of MIL-53(Al) doped with V, when heating from RT in ambient air and in vacuum.[15] Figure 2 shows the results of similar *in situ* XRD experiments. At the start of the experiments, the MOF was at ambient (humid) air conditions. Its XRD pattern matches that reported by Loiseau *et al.*[9] for the **np-h** state. By heating (Figure 2b) a gradual change in the lattice parameters occurs in the 320-350 K range, after which **np** MIL-53(Al) reaches a metastable intermediate state with a decreased unit cell volume with respect to the **np-h** state. TGA (Figure 2a) shows a weight loss of the sample of slightly more than 6% in the same temperature range, while above 350 K the weight loss is considerably slowed down. Indeed, between 350 and 450 K the sample loses less than 1% weight, while XRD reveals that in this range a transition from the intermediate metastable **np** state to **lp** takes place. Our TGA results agree with those for pure MIL-53(Al)[9], but there the water loss of the MIL-53(Al) structure was associated with the **np** to **lp** transition.

Our results strongly suggest that the **np-h** state of MIL-53(Al) dehydrates in a continuous way, leading to a gradual change in lattice parameters, and that the structure is (practically) completely dehydrated before the transition to the **lp** state occurs. The metastable intermediate **np** state may thus be identified as the **np-d** state of MIL-53(Al).

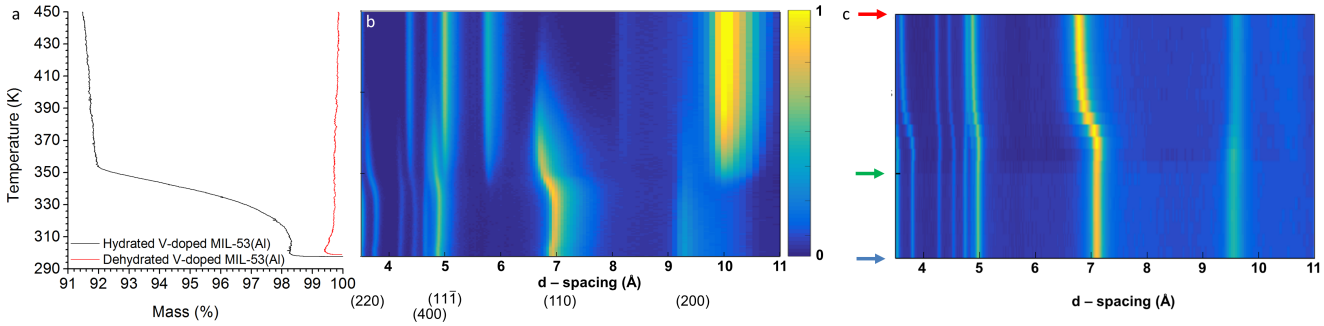

Fig. 2 a: TGA measurements of **np-h** and **np-d** activated V-doped MIL-53(Al) (sample 8) in air. b: Temperature dependence of XRD patterns of activated V-doped MIL-53(Al) (sample 4) in air, λ = 1.54056 Å. 2θ is converted to d-spacing in Å via Bragg's law. Miller indices for all high-intensity peaks are indicated for the **np-h** of MIL-53(Al). The sample was at RT in the **np-h** state. Continuous transition from **np-h** to **np-d** state is observed in a region between 320 and 350 K. The temperature axis is coupled with the temperature axis of the TGA measurement. c: Pressure dependence of the XRD patterns of activated V-doped MIL-53(Al) (sample 4) at RT , λ = 1.54056 Å. 2θ is converted to d-spacing in Å via Bragg's law. Blue arrow indicates t = 0 when the sample was in the **np-h** state in air (1015 mbar). Green arrow indicates moment when pump was switched on (t = 535 s). A continuous transition from the **np-h** to the **np-d** state is observed. At the end of experiment (red arrow, t=1527 s) the pressure p was $\sim$0.08 mbar.

Liu *et al.*[12] previously reported a dehydrated **np** state for MIL-53(Al), obtained by exposing the MOF to high vacuum. Inspired by this, we also followed the MIL-53(Al) state by *in situ* XRD while reducing the pressure. The results of these experiments are summarized in Figure 2c. At the start, the sample was in the **np-h** state at ambient conditions. After switching on the pump (at t = 535 s) the continuous shift of the diffraction peak near 7Å indicates that MIL-53(Al) is dehydrating quite quickly. The total shift in d-spacing observed in this process (0.33$\pm$0.03 Å) is similar to that observed in the *in situ* heating experiment (0.20$\pm$0.07 Å), even though these two experiments are not completely equivalent due to the temperature, and possibly also pressure dependence of the lattice parameters. When the sample is re-exposed to air, the XRD pattern slowly (within 60 min) returns to that of the **np-h** state (not shown). The experiments presented here were performed on MIL-53(Al) samples doped with V, but we checked via experiments on undoped MIL-53(Al) that the results do not depend on the small fraction of V^{III}-OH or V^{IV}=O ions replacing Al-OH in the structure. Lattice parameters for **lp**, **np-d** and **np-h** states determined from our experiments are summarized in Table S1 (ESI†) and compared to literature values for MIL-53(Al) and MIL-53(Ga).

The three states of activated V-doped MIL-53(Al) can also be distinguished via the EPR spectra of

the V^{IV}=O dopant. Figure 3 shows powder EPR spectra for the **lp**, **np-d** and **np-h** state recorded in X-band at RT. All three spectra exhibit the typical EPR spectrum of V^{IV}=O molecular ions (V^{IV} in a $3d^1$ configuration (S=1/2, I=7/2 for the 99.75% abundant ^{51}V). The ^{51}V HF structure is well-resolved and the EPR line widths are narrow, which indicate that the V^{IV}=O ions are well-dispersed in the framework in these samples with low V concentration. As we indicated before[15], the EPR spectra reflect very well the larger deviation from axial symmetry for V^{IV}=O in the **np** states, as compared to the **lp** state, resulting in a larger number of spectral features. The differences in the V^{IV}=O X-band EPR spectra between the two **np** states is more subtle, but still clearly visible. In particular, the linewidth for **np-h** is considerably larger than for **np-d**, whereas the total spectral range of the latter is slightly larger. The differences between these two states become clearer at higher microwave frequencies, as will be discussed in detail in the section 3.3.

3.2 Oxidation state of vanadium in V-doped MIL-53(Al)

Even though a V^{III} dopant salt is used for synthesis, V-doped MIL-53(Al) **as** already exhibits a clear V^{IV}=O related EPR signal in samples with low vanadium concentration (0.5-5 % V). This implies that part of the V^{III} ions were oxidized to V^{IV} during the synthesis.[14] In order to obtain a more quantitative insight in the V-dopant oxidation state distribution in MIL-53(Al) and its evolution throughout the activation processes, XANES experiments were performed and correlated with V^{IV}=O EPR intensity measurements. In Figure 4 a and b, the XANES spectra are shown for samples 5, 6 and 7 in the **as** state, after activation by solvent extraction, and after calcination. In K-edge XANES spectroscopy on vanadium oxides, the main edge energy position (μ_x=0.5) is linearly correlated to the oxidation state of vanadium in the oxide. A correlation curve of the oxidation state as a function of the main edge energy position was made using four reference compounds with increasing vanadium oxidation state: V_2O_3, VO_2, V_6O_{13} and V_2O_5. This curve was then employed to determine the average oxidation state of the V dopant in MIL-53(Al). The obtained average oxidation states are listed in Table 2. On the other hand, the pre-edge peak gives information on the local symmetry at the vanadium site: the peak is absent for sites with inversion symmetry. For **as** samples the pre-edge peak has very low intensity (Figure 4a), while it grows considerably upon activation by solvent extraction, and even further when samples are calcined. In Figure 4 d and e the incorporation sites for V^{III}-OH and V^{IV}=O in MIL-53(Al) are compared. The former site is (close to) inversion symmetric, whereas the latter clearly lacks inversion symmetry in the first coordination shell, since along the c-axis V^{IV} has one O and one OH ligand. Hence, the pre-edge peak intensity may here be considered as a measure for the dopant fraction present as V^{IV}=O. The integrated pre-edge peak intensities are also listed in Table 2.

Figure 4c shows RT EPR spectra of samples 5, 6 and 7, again in **as** and both activated states. For reliable EPR intensity determination, the activated samples were brought to the **lp** state by heating under vacuum to 450 K for 1h and cooling down under vacuum to RT, and EPR spectra were recorded at RT. The EPR intensities were evaluated by double integration of simulated spectra (V^{IV}=O in **as** and **lp** MIL-

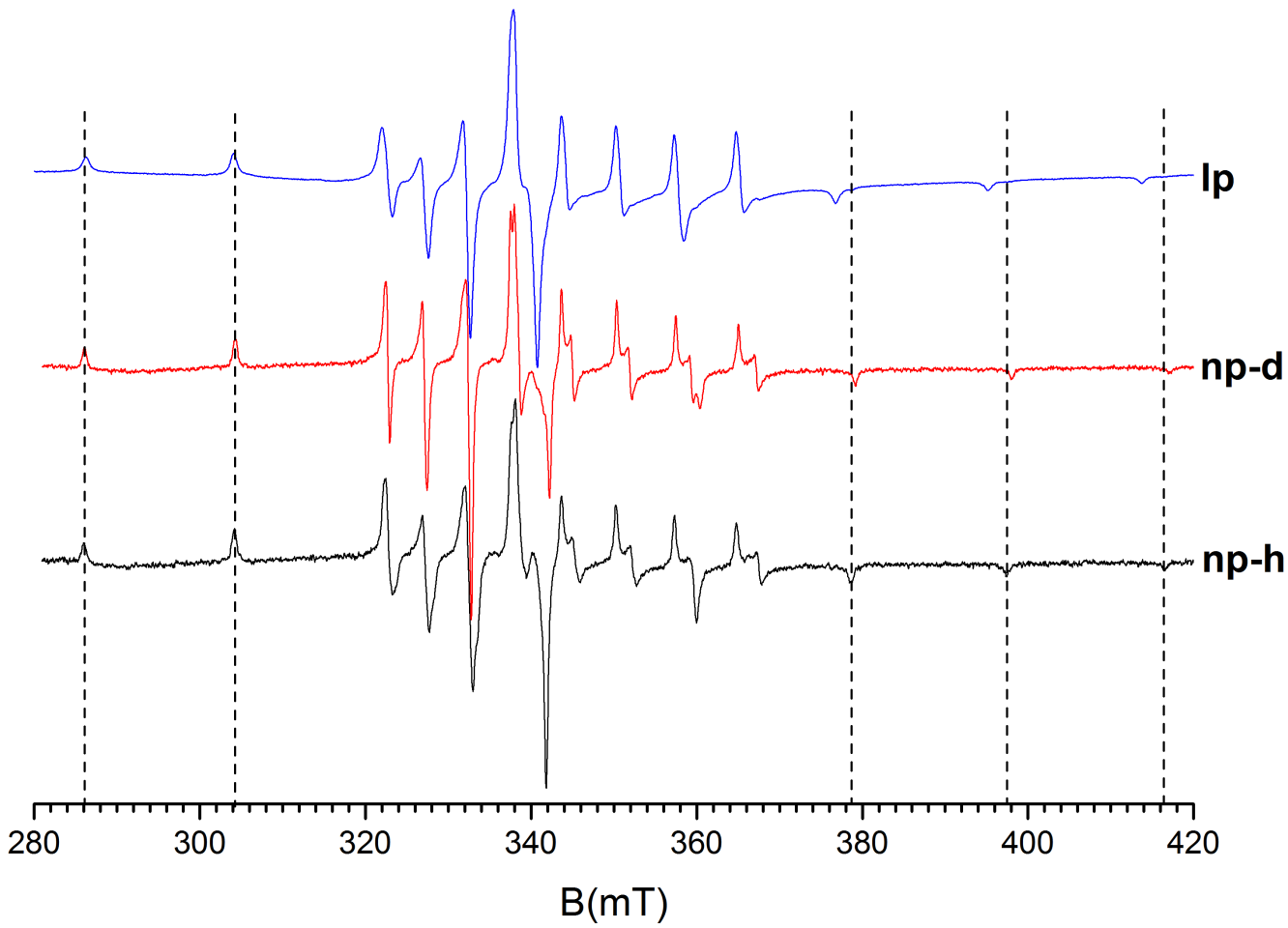

Fig. 3 Experimental X-band powder EPR spectra of activated V-doped MIL-53(Al) in **lp** (sample 1), **np-d** (sample 6) and **np-h** (sample 6) states recorded in N_2 at RT, ν_{MW} = 9.510 GHz. The vertical dashed lines serve as guide for the eye, to highlight changes in the position of the first two and last three lines in the *z*-component (smallest principal *g* and largest principal *A*) hyperfine pattern of the vanadyl spectrum. The intensities of the spectra are normalized.

53(Al)) in order to avoid interfering effects of background signals. The results are presented in Table 2. We observe that activation by solvent extraction already strongly increases the total intensity of the V^{IV} EPR spectrum, although it is mainly aiming at removing unreacted linker molecules from the structure (clearing the pores) and not at oxidizing the dopant. In all three samples investigated, after calcination, which according to the XANES analysis brings (nearly) all V in oxidation state IV, the intensity of the signal grows by at least a factor of three. The limited number of samples studied here suggests that the fraction of dopant directly incorporated as V^{IV}=O decreases with increasing dopant concentration. Although a larger concentration series should be studied to obtain conclusive results, the trend observed here is consistent with earlier results for MIL-47(V)[25] and related V-MOFs (COMOC-3[26], NH_2-MIL-

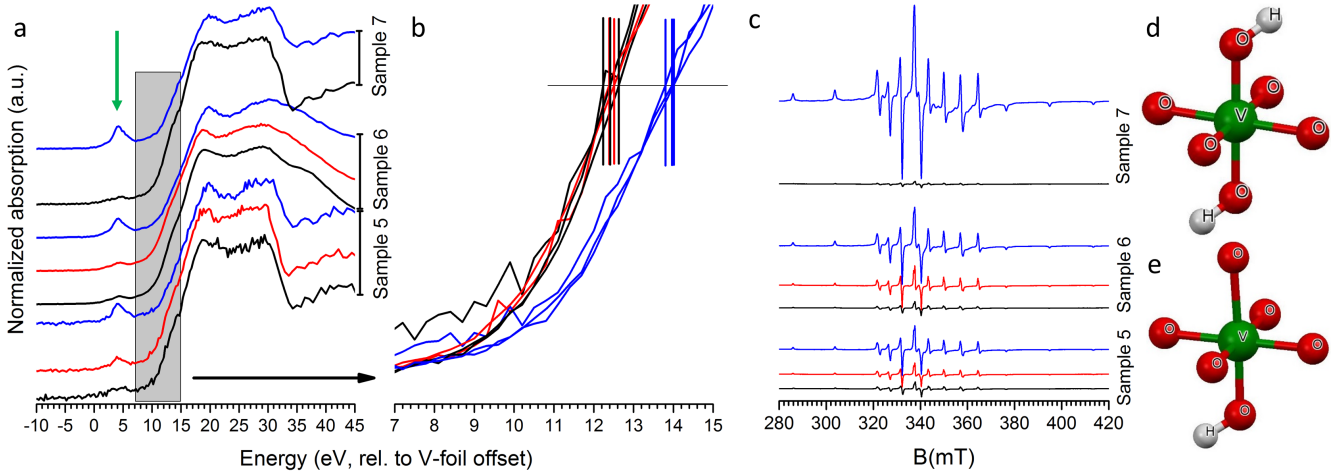

Fig. 4 a: XANES spectra of V-doped MIL-53(Al) sample 5, 6 and 7 in **as** (black), activated by the solvent extraction method (red) and activated by calcination (blue). Spectra are intensity normalized. The grey region is zoomed and shown in Figure 4b. Green arrow indicates pre-edge peak. b: Horizontal and vertical lines represent the main edge energy position (μ_x=0.5) that is linearly correlated to the V oxidation state of each sample. c: RT X-band EPR spectra in vacuum of V-doped MIL-53(Al) sample 5, 6 and 7 **as** (black), activated by the solvent extraction method (red) and activated by calcination (blue). The spectra are normalized to the mass and simulated with the parameters from Table 3 (see section 3.3). The simulated spectrum is double integrated to obtain the approximate number of spins listed in Table 2. d and e: Representation of inversion symmetry and lack of inversion symmetry (respectively) in V-doped MIL-53(Al) (Mercury software used for visualization[24]).

47[27]), where **as** samples exhibit only a very small EPR signal, that grows about two orders of magnitude in intensity after calcination.

3.3 Spin-Hamiltonian analysis of V^{IV} in three states of MIL-53(Al)

Our recent study on V-doped MIL-53(Al) **as**[14] showed that a detailed and accurate spin-Hamiltonian analysis requires a multi-frequency EPR approach. RT EPR spectra of V-doped **lp** MIL-53(Al) were recorded in X, Q and W-band. Figure 5 shows experimental spectra together with simulations. Using a single set of spin-Hamiltonian parameters (Table 3) all spectral features are convincingly reproduced by the simulations for all three bands. The resulting g and $A(^{51}V)$ tensors have non-coincident principal directions. They are very close to those we reported earlier for the **as** state.[14] This could be expected considering the similarities in crystal structure between the **as** and **lp** states of MIL-53(Al). The main differences are found for the γ Euler angle and the linewidth (typically 2-3 times smaller linewidth was found for **lp** state than for **as** state).

The RT EPR spectrum of V-doped MIL-53(Al) in the **np-d** state was recorded in X, Q and J-band. Figure 6 shows experimental spectra together with simulations. Like for **lp**, simulations using a single set of spin-Hamiltonian parameters (Table 4) reproduce the X and Q-band spectra perfectly. The J-band

Table 2 Average oxidation states and pre-edge peak intensity of V-doped MIL-53(Al) determined from XANES measurements for sample 5, 6 and 7 in **as**, activated by the solvent extraction method and activated by calcination compared to V^{IV} ions in the V-doped MIL-53(Al) framework obtained by double integration of EPR spectra. Error on oxidation state is ± 0.4 and EPR intensities $\pm 10\%$.

	Oxidation state	EPR intensity	Pre-edge peak intensity
Sample 5 (0.57 V%)			
as	3.4	90	0
Extraction	3.5	146	0.5
Calcination	4.1	322	0.8
Sample 6 (1.65 V%)			
as	3.4	77	0.35
Extraction	3.5	221	0.5
Calcination	4.2	536	0.61
Sample 7 (4.71 V%)			
as	3.4	33	0.5
Calcination	4.2	1240	0.77

Table 3 Simulation parameter set extracted from multi-frequency EPR spectra at RT of activated V-doped MIL-53(Al) in **lp** and **as** state: g, $A(^{51}V)$ tensor principal values and the Euler angles of the A tensor with respect to the g tensor (tilting angles). The errors are estimated as $\Delta g = \pm 0.00010$, $\Delta A = \pm 1.0$ MHz and $\Delta\alpha$, $\Delta\beta$, $\Delta\gamma = \pm 2^\circ$ for **lp** state. Parameters for **as** are reproduced from Ref.[14], with errors $\Delta g = \pm 0.0010$, $\Delta A = \pm 2.0$ MHz and $\Delta\alpha$, $\Delta\beta$, $\Delta\gamma = \pm 2^\circ$.

	x	y	z	α	β	γ
lp state						
g	1.97243	1.96751	1.93873	0°	11°	0°
A(MHz)	165.6	164.3	495.5			
as state[14]						
g	1.9725	1.9669	1.9391	0°	12°	8°
A(MHz)	163.0	165.0	492.0			

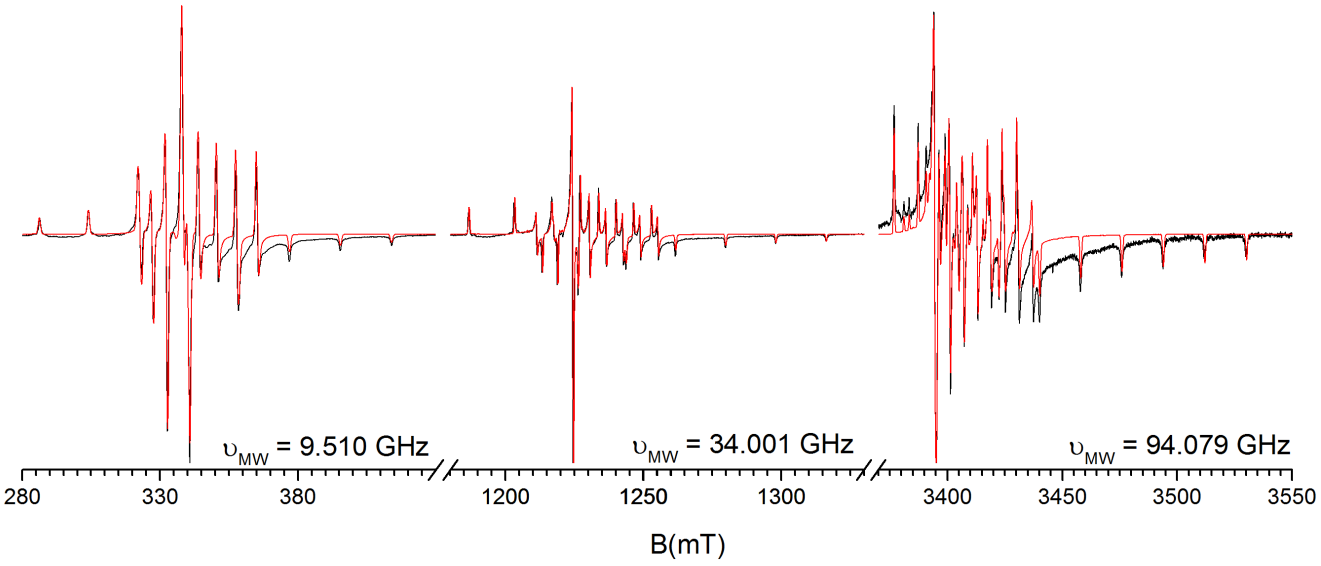

Fig. 5 EPR spectra of activated V-doped MIL-53(Al) in **lp** state at RT in X (sample 1), Q (sample 3) and W-band (sample 2) in 1000 mbar N_2. Experimental spectra are shown in black and simulated spectra with parameters in Table 3 are in red. Spectra are normalized to the same maximum signal height.

Table 4 Simulation parameter set extracted from multi-frequency EPR spectra at RT of activated V-doped MIL-53(Al) in the **np-d** state: g, $A(^{51}V)$ tensor principal values and the Euler angles of the A tensor with respect to the g tensor (tilting angles). The errors are estimated as $\Delta g = \pm 0.00010$, $\Delta A = \pm 1.0$ MHz and $\Delta\alpha$, $\Delta\beta$, $\Delta\gamma = \pm 2°$.

	x	y	z	α	β	γ
np-d state						
g	1.97193	1.96342	1.92922	0°	14°	8°
A(MHz)	165.9	173.0	505.7			

spectrum is also reproduced for the major part, but at low fields an additional spectral component with substructure occurs. Because of its high g value (≈ 1.978) it seems practically excluded that this feature is related to the V^{IV}=O complex observed in X and Q-band. Very probably it is due to a paramagnetic centre with low concentration and rather isotropic spin-Hamiltonian, whose spectrum remains buried under the strong V^{IV}=O spectrum at the lower microwave frequencies. In comparison with those for **as** and **lp**, the g and A tensors for V^{IV}=O in **np-d** MIL-53(Al) are considerably more rhombic. This is already revealed in the X-band spectrum and is also expected when comparing crystallographic data for **np** and **lp** MIL-53(Al).[15]

For the **np-h** state it appeared impossible to simulate spectra simultaneously matching the experiments in X, Q and J-band with only one set of spin-Hamiltonian parameters. In particular in the Q-band spectrum best fit simulations failed to reproduce all resolved spectral features, as illustrated in the ESI†

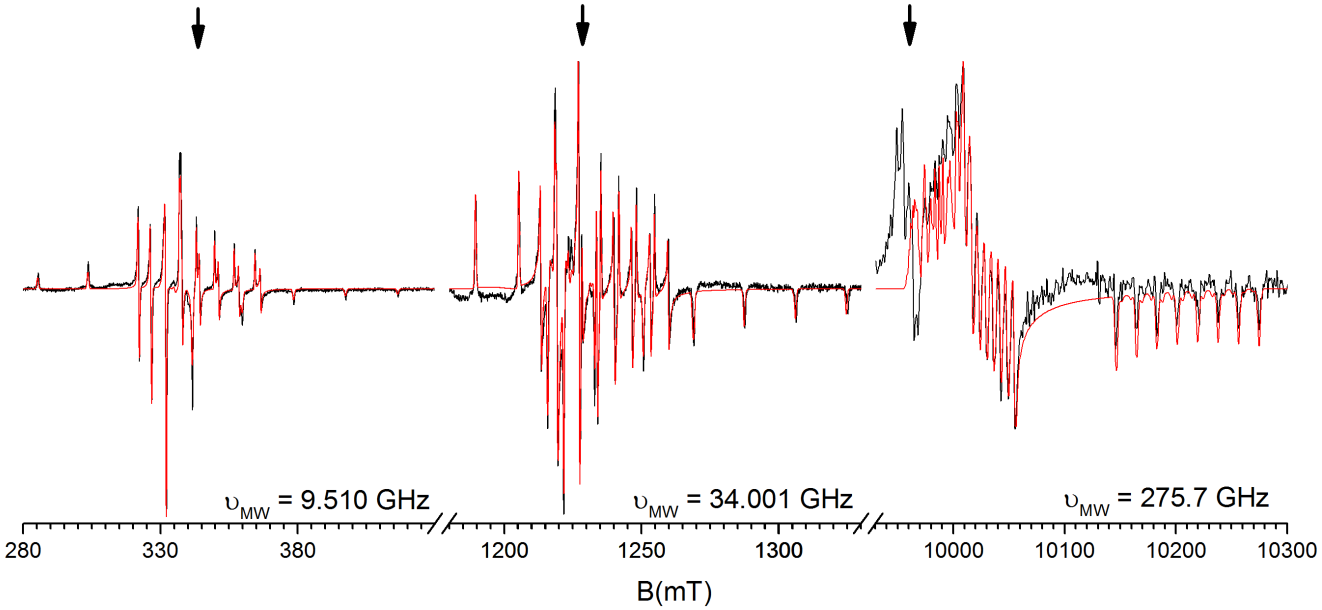

Fig. 6 EPR spectra of activated V-doped MIL-53(Al) in the **np-d** state in X, Q and J-band in vacuum. X and Q-band spectra were recorded at RT while the J-band spectrum was recorded at 325 K. Experimental spectra are shown in black and simulated with parameters from Table 4 in red. Spectra are intensity normalized. Sample 4 was used for all frequencies. Arrows indicate the position where the signal with g = 1.978 observed in J-band would be in all three bands.

(Figure S3, spectrum 7). In the W and J-band spectra, the g_x - g_y region was not sufficiently resolved to allow conclusive fitting. In J-band again an extra spectral component occurred around 9950 mT ($g \approx$ 1.978), further complicating the analysis of the V^{IV}=O spectrum. All these characteristics indicate that at least two (slightly) different V^{IV}=O centres contribute to the EPR spectrum for **np-h** MIL-53(Al). For the **as** state[14] at higher microwave frequencies (W-band) it became obvious that a second V^{IV}=O component (second set of spin-Hamiltonian parameters) was needed for a complete reproduction of the spectra. This approach was also tested here for the **np-h** state. As XRD revealed a gradual change from **np-d** to **np-h** when exposing a sample dried in vacuum conditions to ambient (humid) air, we followed the hydration of **np-d** *in situ* with Q-band EPR measurements monitoring spectra as a function of exposure time to air (Figure S3 of ESI†). A gradual change of the EPR spectrum occurred in the first hours of air exposure. These spectra could be convincingly reproduced by single V^{IV}=O centre simulations with gradually changing g and A tensors (Table S2 of ESI†). The EPR spectrum recorded after 30 h exposure to air was taken as a first component of the finally obtained **np-h**, since that spectrum still clearly exhibited one dominant component. A second component was then found by subtracting the first component from the finally obtained **np-h** EPR spectrum and initial guesses for its spin-Hamiltonian parameters were obtained by fitting the Q-band difference spectrum. Finally, by fitting the EPR spectra for the **np-h** state in all 4 microwave bands simultaneously, satisfactory agreement with experiment was obtained (Figure 7

and Figure S4 of ESI†). The resulting spin-Hamiltonian parameters for the two components are listed in Table 5. Since these parameter sets are only very slightly different, it is perfectly understandable that the two components are not resolved in X-band. Even though the simulated spectra now reproduce (almost) all resolved spectral features in the four bands (except for the extra component in J-band), the calculated two component spectra are not as convincingly matching experiment as the one component simulations for **lp** and **np-d**. The analysis presented here by no means excludes that more than two distinct V-dopant sites are present in the **np-h** state of MIL-53(Al), or that a (quasi) continuous range of different environments for V^{IV}=O exists in this state. A summary of all experimental and simulated spectra in four states and four bands can be found in ESI†, Figure S5.

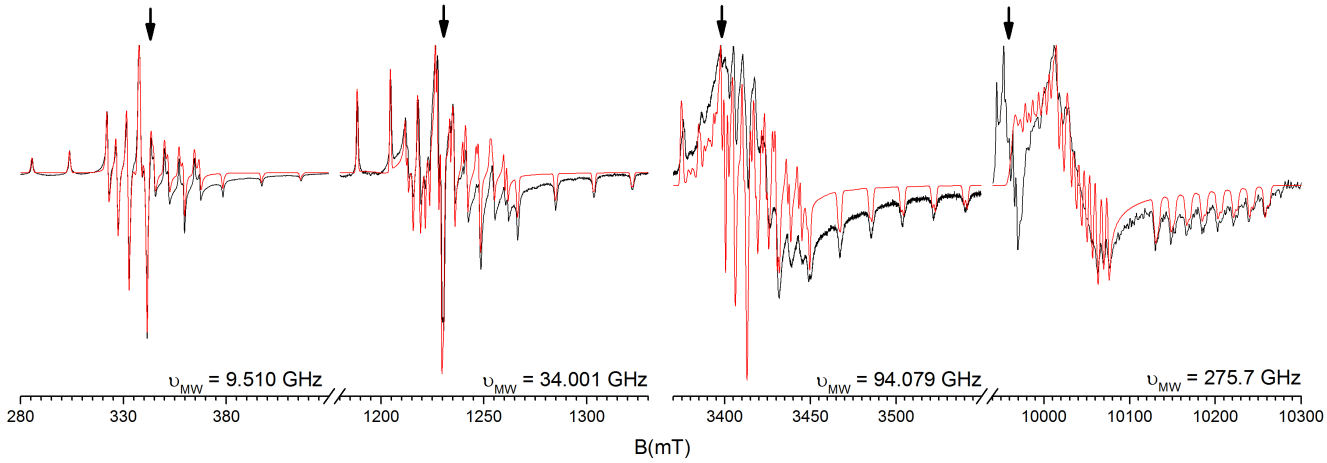

Fig. 7 EPR spectra of activated V-doped MIL-53(Al) in **np-h** state at RT in X (sample 1), Q (sample 1), W (sample 2) in air and J-band (sample 4) in N_2 atmosphere. Experimental spectra are shown in black and simulated spectra with parameters from Table 5 in red. Spectra are normalized in height. The arrows indicate the positions where the signal with g = 1.978 observed in J-band would occur in all four bands.

When recording X and Q-band EPR spectra of V^{IV}=O in **lp** and **np-d** MIL-53(Al) with small modulation amplitude, an additional splitting is observed that can be attributed to the hyperfine interaction with the proton in the OH group of one of the Al^{III} ions neighbouring the V^{IV}=O centre along the metal chains (see ESI† figure S6). On the other hand, ENDOR spectra recorded for the **np-h** state at 10 K reveal interactions with ^{27}Al nuclei (ESI†, Figure S7). These findings explicitly confirm that in all MIL-53(Al) states V^{IV}=O replaces Al^{III}-OH at regular node positions.

3.4 O_2 sensing

In our previous study we reported that when cooling down V-doped MIL-53(Al) in the **lp** state in air to RT, the EPR spectrum broadens due to the interaction with O_2, which is also paramagnetic.[15] This oxygen sensitivity is further explored here. Sample 4 was heated to induce the **lp** state and then cooled down to RT under vacuum. O_2 gas was added into the sample tube in steps of approximately 10 mbar and

Table 5 Simulation parameter set extracted from multi-frequency EPR spectra at RT of activated V-doped MIL-53(Al) in the **np-h** state: g, $A(^{51}\mathrm{V})$ tensor principal values and the Euler angles of the A tensor with respect to the g tensor (tilting angles). The errors are estimated as $\Delta g = \pm 0.0010$, $\Delta A = \pm 1.0$ MHz and $\Delta\alpha, \Delta\beta, \Delta\gamma = \pm 2^\circ$.

	x	y	z	α	β	γ
np-h state						
Component 1						
g	1.9722	1.9623	1.9316	0°	14°	8°
A(MHz)	164.9	174.2	506.4			
Component 2						
g	1.9713	1.9594	1.9324	0°	14°	8°
A(MHz)	162.5	170.9	504.1			

the results of X-band EPR measurements are presented in Figure 8a. Since the EPR spectrum of V-doped MIL-53(Al) extends over a wide field range (160 mT), we zoomed in on its central part. Two effects are clearly observed as a function of oxygen pressure: the height of the EPR signal drops with increasing pressure, and at the same time the spectrum broadens.

With the spin-Hamiltonian parameters for V^{IV}=O in **lp** MIL-53 accurately known (Table 3), simulations (assuming an isotropic Lorentzian line width) have been used to determine the line width with high accuracy, as shown in Figure 8b. The line width increases close-to-linearly with oxygen pressure in the probed range from $0-100$ mbar. Also the signal height (ΔI in Fig. 8c) is monotonously dependent on the O_2 pressure in this range. Both parameters can thus be used to sense oxygen pressure, but the line width evaluation is clearly preferred, since it is independent of sample quantity and instrument parameters. The sensitivity to O_2 pressure is estimated at 5 mbar, comparable to that of some commercially available charcoals for EPR oximetry.[28–30] The sensitivity and ease of line width evaluation of this oxygen sensing system would, however, considerably be improved if the paramagnetic probe ion would exhibit a simpler EPR spectrum. Ti^{III}, with $S = 1/2$ and 87% natural abundance in isotopes with $I = 0$, might present an interesting alternative.

Contrary to the **lp** state, neither the **np-h** nor the **np-d** state exhibit any change in the V^{IV}=O EPR spectrum for O_2 pressures up to 1000 mbar (Fig. 8 d). Although not a priori expected, this result seems in line with the observations of Mishra *et al.*[31] that O_2 can only enter **np** MIL-53(Al) at pressures considerably higher than 1000 mbar.

4 Conclusions

In situ XRD experiments in air, combined with TGA, showed that, starting from ambient conditions, upon heating activated MIL-53(Al) undergoes the following sequence of framework transitions: **np-h** $\rightarrow$ **np-d** $\rightarrow$ **lp**. The transition between the **np-h** and **np-d** states is not abrupt: in the temperature range 320-350 K H_2O is gradually released, as evidenced by a gradual change in the framework lattice parameters. Starting

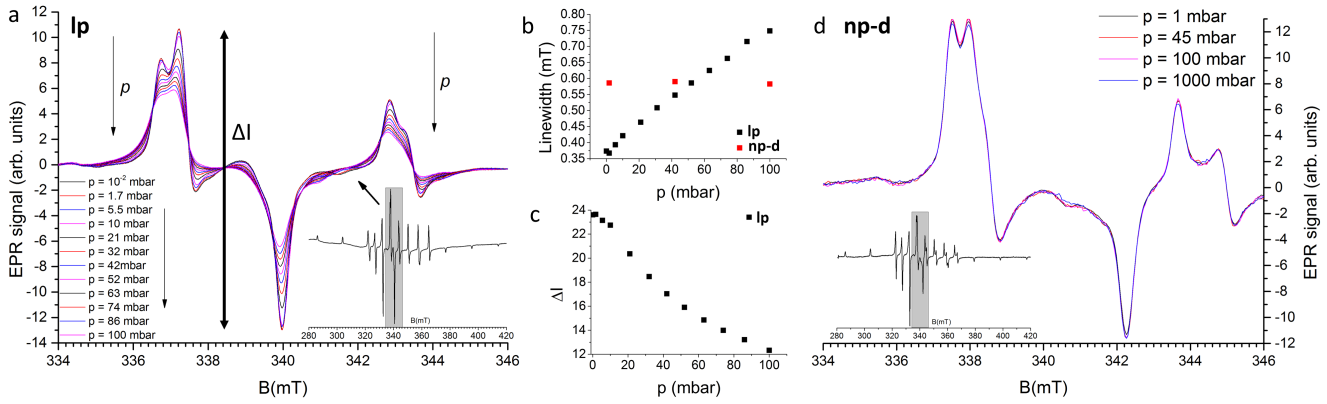

Fig. 8 a: RT X-band EPR spectra (zoomed region) of activated V-doped MIL-53(Al) sample 4 in the **lp** state as a function of O_2 pressure at RT. The inset shows the complete EPR spectrum. The arrows indicate the decrease in peak amplitude and the line broadening with increasing O_2 pressure p. b: Linewidth of the EPR spectra from Figure 8a and Figure 8d as a function of O_2 pressure. The linewidths (full width at half maximum) are obtained from simulations with the parameters from Table 3 for the **lp** and Table 4 for the **np-d** state. c: Difference in amplitude between two EPR peaks (337 mT and 340 mT) of the **lp** state as a function of O_2 pressure. d: RT X-band EPR spectra (zoomed region) of activated V-doped MIL-53(Al) sample 4 in the **np-d** state as a function of O_2 pressure at RT. The inset shows the complete EPR spectrum.

from **np-h** MIL-53(Al), the **np-d** state can also quite easily be obtained at RT by reducing pressure. The EPR spectra of V^{IV}=O dopant centres appear excellent probes to discriminate between the **as**, **np-h**, **np-d** and **lp** states of this MOF.

XANES and EPR intensity measurements provided consistent information on the oxidation state of the V dopant in MIL-53(Al). Even though $V^{III}Cl_3$ is used as a dopant salt, a small fraction of the dopant is already present in the V^{IV} state immediately after synthesis. Both solvent extraction and calcination activation procedures increase the V^{IV} fraction ; calcination makes the III→IV valence state transition (practically) complete.

The spin-Hamiltonian analysis of the V^{IV}=O centres in the three different states of activated V-doped MIL-53(Al) revealed that, like for the **as** state, the g and ^{51}V A tensor axes are tilted with respect to each other. The spin-Hamiltonian parameters of the **lp** and **as** states are strikingly close which can be explained by a similar wide pore crystal structure. The multi-frequency EPR spectra of V-doped MIL-53(Al) in the **lp** and **np-d** states were convincingly reproduced with only one set of parameters, while this appeared impossible for the **np-h** state. The presence of H_2O in the framework pores produces (at least two) different environments for the V^{IV}=O paramagnetic centres, which is reflected in slightly different EPR spectra.

The EPR spectrum of activated V-doped MIL-53(Al) in the **lp** state is found to be sensitive to oxygen. The close-to-linear dependence of the EPR linewidth on the O_2 pressure opens perspectives for applications in oxygen sensing, with a sensitivity of a few mbar. Remarkably, the EPR spectra of V-doped MIL-53(Al)

in the **np-h** and **np-d** states do not exhibit such broadening, very probably because O_2 cannot enter the framework in these states.

Conflicts of interest

There are no conflicts of interest to declare.

Acknowledgments

The authors gratefully thank the Research Foundation Flanders (FWO-Vlaanderen) for financially supporting this work (Grant No. G0048.13N). I. Nevjestić acknowledges support by the Ghent University Special Research Fund (BOF, Grant No. BOF16/DC1/027). K. Leus acknowledges support by Ghent University BOF postdoctoral grant 01P06813T and the GOA Grant 01G00710. P. Tack acknowledges the Agency for Innovation by Science and Technology (IWT, grant 121289). Additionally, the authors would like to acknowledge the DUBBLE beamline (BM26A, ESRF, Grenoble, France) staff Stephen Bauters and Dipanjan Banerjee for their assistance during the beamtime of XANES measurements. Jevgenij Kusakovskij (Ghent University) is gratefully acknowledged for help with the EPR simulations and Claire Murray (Diamond Light Source, synchrotron facility, Didcot UK) for XRD Lebail refinements.

References

1 X. Lin, N. R. Champness and M. Schröder, in *Hydrogen, Methane and Carbon Dioxide Adsorption in Metal-Organic Framework Materials*, ed. M. Schröder, Springer Berlin Heidelberg, Berlin, Heidelberg, 2010, pp. 35–76.

2 M. P. Suh, H. J. Park, T. K. Prasad and D.-W. Lim, *Chemical Reviews*, 2012, **112**, 782–835.

3 J.-R. Li, R. J. Kuppler and H.-C. Zhou, *Chemical Society Reviews*, 2009, **38**, 1477–1504.

4 Z. Hu, B. J. Deibert and J. Li, *Chemical Society Reviews*, 2014, **43**, 5815–5840.

5 L. E. Kreno, K. Leong, O. K. Farha, M. Allendorf, R. P. Van Duyne and J. T. Hupp, *Chemical Reviews*, 2012, **112**, 1105–1125.

6 K. Leus, M. Vandichel, Y.-Y. Liu, I. Muylaert, J. Musschoot, S. Pyl, H. Vrielinck, F. Callens, G. B. Marin, C. Detavernier, P. V. Wiper, Y. Z. Khimyak, M. Waroquier, V. V. Speybroeck and P. V. D. Voort, *Journal of Catalysis*, 2012, **285**, 196–207.

7 J. Lee, O. K. Farha, J. Roberts, K. A. Scheidt, S. T. Nguyen and J. T. Hupp, *Chemical Society Reviews*, 2009, **38**, 1450–1459.

8 J. Della Rocca, D. Liu and W. Lin, *Accounts of Chemical Research*, 2011, **44**, 957–968.

9 T. Loiseau, C. Serre, C. Huguenard, G. Fink, F. Taulelle, M. Henry, T. Bataille and G. Férey, *Chemistry-a European Journal*, 2004, **10**, 1373–1382.

10 P. Rallapalli, D. Patil, K. P. Prasanth, R. S. Somani, R. V. Jasra and H. C. Bajaj, *Journal of Porous Materials*, 2010, **17**, 523–528.

11 C. Serre, F. Millange, C. Thouvenot, M. Noguès, G. Marsolier, D. Louër and G. Férey, *Journal of the American Chemical Society*, 2002, **124**, 13519–13526.

12 Y. Liu, J.-H. Her, A. Dailly, A. J. Ramirez-Cuesta, D. A. Neumann and C. M. Brown, *Journal of the American Chemical Society*, 2008, **130**, 11813–11818.

13 C. Volkringer, T. Loiseau, N. Guillou, G. Férey, E. Elkaim and A. Vimont, *Dalton Transactions*, 2009, 2241–2249.

14 I. Nevjestić, H. Depauw, K. Leus, V. Kalendra, I. Caretti, G. Jeschke, S. Van Doorslaer, F. Callens, P. Van Der Voort and H. Vrielinck, *ChemPhysChem*, 2015, **16**, 2968–2973.

15 I. Nevjestić, H. Depauw, K. Leus, G. Rampelberg, C. A. Murray, C. Detavernier, P. Van Der Voort, F. Callens and H. Vrielinck, *The Journal of Physical Chemistry C*, 2016, **120**, 17400–17407.

16 H. Depauw, I. Nevjestić, J. De Winne, G. Wang, K. Haustraete, K. Leus, A. A. Verberckmoes, C. Detavernier, F. Callens, E. De Canck, H. M. Vrielinck and P. Van Der Voort, *Chem. Commun.*, 2017, –.

17 J. P. S. Mowat, V. R. Seymour, J. M. Griffin, S. P. Thompson, A. M. Z. Slawin, D. Fairen-Jimenez, T. Duren, S. E. Ashbrook and P. A. Wright, *Dalton Transactions*, 2012, **41**, 3937–3941.

18 F. Millange, N. Guillou, R. I. Walton, J.-M. Greneche, I. Margiolaki and G. Férey, *Chemical Communications*, 2008, 4732–4734.

19 R. A. Serway and S. A. Marshall, *The Journal of Chemical Physics*, 1967, **46**, 1949–1952.

20 H. Blok, J. A. J. M. Disselhorst, S. B. Orlinskii and J. Schmidt, *Journal of Magnetic Resonance*, 2004, **166**, 92–99.

21 S. Stoll and A. Schweiger, *Journal of Magnetic Resonance*, 2006, **178**, 42–55.

22 M. Tinkham and M. W. P. Strandberg, *Physical Review*, 1955, **97**, 937–951.

23 S. Nikitenko, A. M. Beale, A. M. J. van der Eerden, S. D. M. Jacques, O. Leynaud, M. G. O'Brien, D. Detollenaere, R. Kaptein, B. M. Weckhuysen and W. Bras, *Journal of Synchrotron Radiation*, 2008, **15**, 632–640.

24 C. F. Macrae, I. J. Bruno, J. A. Chisholm, P. R. Edgington, P. McCabe, E. Pidcock, L. Rodriguez-Monge, R. Taylor, J. van de Streek and P. A. Wood, *Journal of Applied Crystallography*, 2008, **41**, 466–470.

25 O. Kozachuk, M. Meilikhov, K. Yusenko, A. Schneemann, B. Jee, A. V. Kuttatheyil, M. Bertmer, C. Sternemann, A. Pöppl and R. A. Fischer, *European Journal of Inorganic Chemistry*, 2013, **2013**, 4546–4557.

26 Y.-Y. Liu, K. Leus, M. Grzywa, D. Weinberger, K. Strubbe, H. Vrielinck, R. Van Deun, D. Volkmer, V. Van Speybroeck and P. Van Der Voort, *European Journal of Inorganic Chemistry*, 2012, **2012**, 2819–2827.

27 K. Leus, S. Couck, M. Vandichel, G. Vanhaelewyn, Y.-Y. Liu, G. B. Marin, I. V. Driessche, D. Depla, M. Waroquier, V. V. Speybroeck, J. F. M. Denayer and P. V. D. Voort, *Physical Chemistry Chemical Physics*, 2012, **14**, 15562–15570.

28 B. F. Jordan, C. Baudelet and B. Gallez, *Magnetic Resonance Materials in Physics, Biology and Medicine*, 1998, **7**, 121–129.

29 M. Kržič, M. Šentjurc and J. Kristl, *Journal of Controlled Release*, 2001, **70**, 203–211.

30 J. A. O'Hara, F. Goda, K. J. Liu, G. Bacic, P. J. Hoopes and H. M. Swartz, *Radiation Research*, 1995, **144**, 222–229.

31 P. Mishra, S. Edubilli, H. P. Uppara, B. Mandal and S. Gumma, *Langmuir*, 2013, **29**, 12162–12167.